JOURNAL OF AGRICULTURAL AND FOOD CHEMISTRY

Preparation and Characterization of Chitosan-Based Nanocomposite Films with Antimicrobial Activity

JONG-WHAN RHIM,*,† SEOK-IN HONG,§ HWAN-MAN PARK,# AND PERRY K. W. NG⊥

Department of Food Engineering, Mokpo National University, 61 Dorimri, Chungkyemyon, Muangun 534-729, Chonnam, Republic of Korea; Korea Food Research Institute, San 46-1, Baekhyun-dong, Bundang-gu, Seongnam-si 463-746, Kyonggi-do, Republic of Korea; Composite Materials and Structures Center, 2100 Engineering Building, Michigan State University, East Lansing, Michigan 48824-1226; and Department of Food Science and Human Nutrition, Michigan State University, East Lansing, Michigan 48824-1224

Four different types of chitosan-based nanocomposite films were prepared using a solvent-casting method by incorporation with four types of nanoparticles, that is, an unmodified montmorillonite (Na-MMT), an organically modified montmorillonite (Cloisite 30B), a Nano-silver, and a Ag-zeolite (Ag-Ion). X-ray diffraction patterns of the nanocomposite films indicated that a certain degree of intercalation was formed in the nanocomposite films, with the highest intercalation in the Na-MMT-incorporated films followed by films with Cloisite 30B and Ag-Ion. Scanning electron micrographs showed that in all of the nanocomposite films, except the Nano-silver-incorporated one, nanoparticles were dispersed homogeneously throughout the chitosan polymer matrix. Consequently, mechanical and barrier properties of chitosan films were affected through intercalation of nanoparticles, that is, tensile strength increased by 7−16%, whereas water vapor permeability decreased by 25−30% depending on the nanoparticle material tested. In addition, chitosan-based nanocomposite films, especially silver-containing ones, showed a promising range of antimicrobial activity.

KEYWORDS: Chitosan-based film; nanocomposite; montmorillonite; Nano-silver; Ag-zeolite; antimicrobial activity

INTRODUCTION

In the past half century, synthetic petroleum-based polymers have been widely used in a variety of packaging materials but have become a major source of waste disposal problems due to their poor biodegradability. With increasing demand of consumers for high-quality foods and concerns about limited natural resources and the environment, the use of renewable resources to produce edible or biodegradable packaging materials that can improve product quality and reduce waste disposal problems are being explored. One of the approaches is to use renewable biopolymers such as polysaccharides, proteins, lipids, and their composites, derived from plant and animal resources (*1*−*4*).

Biopolymer-based edible films and coatings are intended to function as barriers against moisture, oxygen, flavor, aroma, and oil, thereby improving food quality and enhancing the shelf life of food products (*5*). They may also provide physical protection to foods, reducing bruising and breakage, thus improving food integrity. Furthermore, biopolymer films are excellent vehicles for incorporating a wide variety of additives, such as antioxidants, antifungal agents, antimicrobials, colors, and other nutrients (*5*−*10*). In particular, biopolymer-based antimicrobial films have been attracting much attention from the food industry with their potential application for a variety of foods including meat, fish, poultry, cereals, cheese, fruits, and vegetables (*8*, *11*−*13*).

However, the use of biopolymer films with their combined properties has been restricted due to their inherent water sensitivity and relatively low stiffness and strength, especially in moist environments (*1*−*4*). Many research studies have focused on improving the physical properties of biopolymer-based films by decreasing the hydrophilicity and improving the mechanical properties. Hydrophobic materials such as neutral lipids, fatty acids, or waxes have been added to improve the moisture barrier properties of biopolymer films (*14*−*20*).

Various physical means, such as UV- or γ-irradiation, ultrasonic treatment, and heat-curing (*1*, *21*−*23*), and chemical means, such as adjustment of pH, chemical modification (*24*, *25*), and addition of cross-linking agents (*26*), have been tested to modify the properties of biopolymer-based films by inducing inter- or intramolecular cross-linking in the polymer matrix.

* Author to whom correspondence should be addressed (telephone +82-61-450-2423; fax +82-61-454-1521; e-mail jwrhim@mokpo.ac.kr).
† Mokpo National University.
§ Korea Food Research Institute.
# Composite Materials and Structure Center, Michigan State University.
⊥ Department of Food Science and Human Nutrition, Michigan State University.

10.1021/jf060658h CCC: $33.50
Published on Web 07/06/2006

Another possible approach to modifying biopolymer film properties is to make hybrid films with organic polymers and nanosized clay minerals such as layered silicates, which are known as nanocomposite films (*27*−*30*). Nanocomposite films consisting of inorganic nanolayers of layered silicate, such as montmorillonite (MMT) clay and organic polymers, have recently evoked intense research interest in the material and polymer science areas (*29*, *31*−*33*). Usually, polymer/clay nanocomposites comprise an organic/inorganic hybrid polymer matrix containing platelet-shaped clay particles that have sizes in the order of a few nanometers thick and several hundred nanometers long. Partly because of their high aspect ratios and high surface area, the clay particles, if properly dispersed in the polymer matrix at a loading level of 1−5 wt %, impart unique combinations of physical and chemical properties that make these nanocomposites attractive for making films and coatings for a variety of industrial applications. Examples of such property enhancements include decreased permeability to gases and liquids, better resistance to solvents, increased thermal stability, and improved mechanical properties (*29*, *31*). Moreover, biodegradability is retained; that is, after final degradation, only inorganic, natural minerals (clay) will be left (*34*, *35*).

Although numerous research works on polymer−clay nanocomposites have been performed, the matrices of these nanocomposites have mainly been synthetic polymers (*29*, *31*). The literature available for natural biopolymer-based nanocomposite materials is limited (*32*, *33*). In addition, limited studies on antimicrobial films based on natural biopolymer nanocomposites were found in the literature (*36*, *37*). The overall objective of the present study was to develop biodegradable antimicrobial bionanocomposite films with acceptable properties for applications in food packaging using biopolymer such as chitosan, as well as Nano-silver, silver zeolite, and nanoscale layered silicates.

MATERIALS AND METHODS

Materials. Chitosan (CS-001, viscosity of 110 cP in a 1% acetic acid solution at 25 °C and degree of deacetylation of 90%) was obtained from Samsung Chitopia (Seoul, Korea). A pristine sodium montmorillonite (Na-MMT, Nanomer PGW, lot PC-243-99, 120 mmol/100 g CEC) was obtained from Nanocore Inc. (Arlington Heights, IL), and organically modified MMT (Cloisite 30B) was purchased from Southern Clay Co. (Gonzales, TX). The ammonium cation of Cloisite 30B is reported to be methyl tallow bis(2-hydroxyethyl) quarternary ammonium. Nano-silver and silver zeolite (Ag-Ion) were obtained from Nano Bio Co. Ltd. (Seoul, Korea) and AgION Technologies, Inc. (Wakefield, MA), respectively. Nano-silver is a dark gray particle composed of 99.2% silver, 0.4% water, and others, with the silver component having a particle size of 76.8 ± 10 nm. Ag-Ion is a mixture of sodium aluminosilicate (zeolite, >75 wt %), silver (2.1−2.8 wt %), zinc (14 wt %), and ammonium, of which the mean particle size distribution is <5.0 μm. Analytical grade glycerin was purchased from J. T. Baker (Mallinckrodt Baker, Inc., Phillipsburg, NJ).

Preparation of Films. Chitosan films were prepared according to the method of Rhim et al. (*38*). Four grams of chitosan powder was dissolved in a constantly stirred mixture of 1% (v/v) acetic acid aqueous solution (200 mL) and glycerin (1.0 g) by heating for ≈20 min at 90 °C using a hot plate. The dissolved film solution was strained through eight layers of cheesecloth to remove undissolved debris and then cast onto a leveled Teflon-coated glass plate (24 × 30 cm) framed at four sides. The castings were dried at ambient conditions (≈23 °C) for ≈48 h and then peeled off the glass plates.

In addition, chitosan-based nanocomposite films were prepared by reinforcement with four different types of nanoparticles, such as Na-MMT, Cloisite 30B, Nano-silver, or Ag-zeolite. First, 5 or 20% (for Ag-Ion only) of each type of nanoparticle (w/w, relative to chitosan on a dry basis) was dispersed in a 1% acetic acid solution (200 mL) by vigorous mixing for 1 h using a magnetic stirrer and then sonicated for 30 min at 60 °C in a bath-type ultrasound sonicator (FS14H, Fisher Scientific) to obtain a nanoparticle solution. Four grams of chitosan powder was then dissolved into the nanoparticle solution after the addition of 1 g of glycerin, and all was heated for ≈20 min at 90 °C using a hot plate mixer. The solution was sonicated for an additional 10 min at 60 °C, after which the solution was strained and cast following the same procedure as for the preparation of chitosan film.

All of the films were cut into 7 × 7, 2 × 2, and 2.54 × 15 cm sized pieces for the measurement of water vapor permeability (WVP), water solubility (WS), and tensile strength (TS) along with elongation at break (*E*), respectively.

Film Thickness and Conditioning. Film thickness was measured to the nearest 0.01 mm using a hand-held micrometer (dial thickness gauge 7301, Mitutoyo). Five thickness measurements were taken on each tensile testing specimen along the length of the rectangular strip, and the mean value was used in TS calculation. Similarly, five measurements were taken on each water vapor permeability specimen, one at the center and four around the perimeter, and the mean values were used in calculating WVP. All film samples were preconditioned for at least 48 h in a constant-temperature humidity chamber set at 25 °C and 50% relative humidity before testing.

Color and Transparency. Color values of the films were measured with a CR-300 Minolta Chroma Meter (Minolta Camera Co., Ltd., Osaka, Japan). Films were placed on a white standard plate (calibration plate CR-A43), and the Hunter *Lab* color scale was used to measure color. Total color difference (ΔE) was calculated as

$$\Delta E = (\Delta L^2 + \Delta a^2 + \Delta b^2)^{0.5}$$

where $\Delta L = L_{standard} - L_{sample}$, $\Delta a = a_{standard} - a_{sample}$, and $\Delta b = b_{standard} - b_{sample}$. Standard values for the white plate were $L = 96.86$, $a = -0.02$, and $b = 1.99$, respectively. Five measurements were taken on each film, one at the center and four around the perimeter, and the mean values were used.

Transparency of the films was determined by measuring the percent transmittance at 660 nm using a UV−visible spectrophotometer (Lambda 25, Perkin-Elmer Instruments, Norwalk, CT).

Tensile Properties. TS and *E* of each film-type sample were determined with an Instron Universal Testing Machine (model 5565, Instron Engineering Corp., Canton, MA). Rectangular specimens (2.54 × 15 cm) were cut using a precision double-blade cutter (model LB.02/A, Metrotec, S.A., San Sebastian, Spain). Initial grip separation was set at 50 mm, and cross-head speed was set at 50 mm/min. The TS and *E* measurements for each type of film were taken as follows: three sheets of each film type were used, with seven specimens cut from each sheet of film; thus, the measurements were done on a total of 21 specimens per each film type, with the mean values for TS and *E* reported for each sample.

Water Vapor Permeability. WVP ($g \cdot m/m^2 \cdot s \cdot Pa$) was calculated as

$$WVP = (WVTR \times l)/\Delta p$$

where WVTR was the measured water vapor transmission rate ($g/m^2 \cdot s$) through a film, l was the mean film thickness (m), and Δp was the partial water vapor pressure difference (Pa) across the two sides of the film. WVTR was determined gravimetrically using a modified ASTM method E 96-95. In calculating WVP, the effect of the resistance of the stagnant air layer between the film underside and the surface of the water in the cup was corrected for using the method of Gennadios et al. (*39*).

Contact Angle of Water. A contact angle analyzer (model Phoenix 150, Surface Electro Optics Co. Ltd., Kunpo, Korea) was used to measure the contact angle of water in air on the surface of chitosan and chitosan-based nanocomposite films. A film sample (3 × 10 cm) was glued on a movable sample stage (black Teflon-coated steel, 7 × 11 cm) and leveled horizontally; then a drop of ≈10 μL of distilled water was placed on the surface of the film using a microsyringe. The contact angles on both sides of the drop were measured to ensure symmetry and horizontal level.

Table 1. Surface Color and Transmittance of Chitosan-Based Nanocomposite Films[a]

film type	*L*	*a*	*b*	ΔE	T_{660}
neat chitosan	85.8 ± 0.0a	−0.9 ± 0.1b	2.7 ± 0.3d	11.2 ± 0.1d	93.2 ± 0.2a
Na-MMT	85.3 ± 0.2b	−1.7 ± 0.1c	7.2 ± 0.7a	12.8 ± 0.4c	92.8 ± 0.6a
Cloisite 30B	85.3 ± 0.2b	−1.7 ± 0.1c	6.3 ± 0.3b	12.4 ± 0.3c	92.5 ± 0.2a
Nano-silver	66.8 ± 0.4d	−0.2 ± 0.0a	4.5 ± 0.1c	30.1 ± 0.4a	57.2 ± 7.8b
Ag-Ion	81.7 ± 0.2c	−0.2 ± 0.2a	7.9 ± 0.5a	16.4 ± 0.4b	91.1 ± 0.2a

[a] Means of three replicates ± standard deviation. Any two means in the same column followed by the same letter are not significantly different from each other ($P > 0.05$) by Duncan's multiple-range test. *L*, *a*, and *b* are Hunter *L*, *a*, *b* values; ΔE is total color difference; T_{660} is transmittance at 660 nm.

Water Solubility. WS of each film was determined as the percentage of film dry matter solubilized after 1 h of immersion in distilled water. Three randomly selected 2 × 2 cm samples from each type of film were first dried at 105 °C for 24 h to determine the weight of the initial dry matter. An additional three pieces of weighed film were placed in a 50 mL beaker containing 30 mL of distilled water. Beakers were covered with Parafilm (American National Can, Greenwich, CT) and stored in an environmental chamber at 25 °C for 1 h with occasional, gentle swirling. Undissolved dry matter was determined by removing the film pieces from the beakers, gently rinsing all pieces with distilled water, and then oven-drying them (105 °C, 24 h).

X-ray Diffraction (XRD). The structure of the nanoparticles in the polymer matrix was evaluated with XRD measurements. A Rigaku 200B X-ray diffractometer (45 kV, 100 mA) equipped with Cu Kα radiation with a wavelength 0.1546 nm and a curved graphite crystal monochromator at a scanning rate of 0.5°/min was used for this purpose.

Scanning Electron Microscopy (SEM). The morphology of the films was examined on their fractured surfaces, obtained after cutting dried film samples with a paper-cutter, using a scanning electron microscope (JSM-6400 scanning microscope, JEOL). The samples of chitosan film and nanocomposite films with Na-MMT and Cloisite 30B were sputter-coated with gold using a microscope sputter coater (emscope, SC500, Quorum Technologies, East Sussex, U.K.) for 1 min at 20 mA and 15 kV, and the samples of nanocomposite films with Nano-silver and Ag-Ion were carbon-coated using a C-string evaporator (Erest F. Fullam, Latham, NY) with an arc voltage of 20 kV, prior to examination.

Antimicrobial Activity. The antimicrobial activity of chitosan and chitosan-based nanocomposite films was tested qualitatively and quantitatively by an inhibition zone method and a viable cell count method, respectively. In both methods, four different food pathogenic bacteria including *Staphylococcus aureus* ATCC-14458, *Leuconostoc monocytogenes* ATCC-19111, *Salmonella typhimurium* ATCC-14028, and *Escherichia coli* O157:H7 ATCC-11775 were used for testing the antimicrobial activity of the films. The cells of *S. aureus* and *L. monocytogenes* were grown on brain heart infusion (BHI) agar (Difco Laboratories, Detroit, MI) and incubated at 37 °C for 2 days. Both strains of *S. typhimurium* and *E. coli* O157:H7 were cultivated on tryptic soy (TS) agar (Difco Lab) at 30 °C for 2 days. All of the stock cultures were stored at 4 °C.

For the qualitative measurement of antimicribial activity, the film samples were punched to make disks (diameter = 6 mm), and the antimicrobial activity was determined using a modified agar diffusion assay (disk test). The plates were examined for possible clear zones after incubation at 37 °C for 2 days. The presence of any clear zone that formed around the film disk on the plate medium was recorded as an indication of inhibition against the microbial species.

The quantitative antimicrobial activity of the films was determined using a viable cell count method on the test pathogenic bacteria. Film samples were cut into square pieces (10 × 10 cm) and placed in individual sterile flasks to be used in the test for microbial inhibition. Two Gram-positive bacteria, *S. aureus* and *L. monocytogenes*, were separately grown in BHI broth (Difco) and incubated aerobically for 16 h at 37 °C. Another two Gram-negative bacteria, *S. typhimurium* and *E. coli* O157:H7, were separately cultivated in TS broth (Difco) at 30 °C for 16 h. Each 30 mL tube of bacterial cell culture was then centrifuged for 5 min at 4 °C and 7000*g*, decanted, washed with 0.1% peptone (Difco), centrifuged for 5 min, and decanted. The cell pellet was placed into 100 mL of BHI or TS broth and diluted to 10% of the original broth concentration with 900 mL of sterile distilled water to obtain an inoculum of ≈$(1.0-2.5) \times 10^6$ colony-forming units (CFU)/mL. Then, 100 mL of the inoculum was aseptically added to each of the flasks containing the sample films. For each type of bacteria, an inoculum of cell suspension in a flask with no film sample was used as a control. The flasks were put on an orbital shaker and rotated at 50 rpm and 30 °C. Aliquots of 0.1 mL of cell suspension were periodically taken from the flasks, diluted serially with 0.1% peptone solution, and plated in duplicate on BHI agar for *S. aureus* and *L. monocytogenes* cells or on TS agar for *S. typhimurium* and *E. coli* O157:H7 cells. The plates were incubated in an aerobic chamber for 2 days at 37 °C for BHI agar and at 30 °C for TS agar. The number of colonies on each plate was counted and reported as CFU per milliliter.

Statistical Analysis. Measurements of each property were triplicated for color, TS, *E*, WVP, and WS as well as the microbial test with individually prepared and cast films as the replicated experimental units. Statistics on a completely randomized design were determined using the General Linear Models procedure in the SAS program (SAS Institute Inc.). Mean property values were separated ($P < 0.05$) with Duncan's multiple-range test.

RESULTS AND DISCUSSION

Apparent Film Properties. Chitosan and chitosan-based nanocomposite films were flexible and free-standing. All of the films were as tough and as smooth-surfaced as cellophane. **Table 1** shows Hunter *L*, *a*, *b* color values, total color difference (ΔE), and transmittance (T_{660}) of the films. Except for the chitosan/Nano-silver nanocomposite film, all of the films were transparent, with a slight yellowish tint in the neat chitosan film, chitosan/Na-MMT, and chitosan/Cloisite 30B nanocomposite films and with a slight brownish tint in the chitosan/Ag-Ion nanocomposite film. However, the chitosan/Nano-silver film was gray in surface color and semitransparent, which was indicated by significantly ($P < 0.05$) lower whiteness (lower Hunter *L*) value, higher redness (higher Hunter *a*) value, and consequently higher total color difference value (ΔE) of the chitosan/Nano-silver film. Although T_{660} values for three of the nanocomposite films were decreased slightly (except for chitosan/Nano-silver films) relative to that of the chitosan film, these decreases were not significant ($P > 0.05$). This was probably due to the fact that in these three films the nanoparticles were evenly distributed through the polymer matrix. Because layered silicates are just 1 nm thick when single layers are dispersed in a polymer matrix, the resulting nanocomposite is optically clear in visible light (*31*). Many researchers have also found that the transparency of nanocomposites, such as poly(vinyl alcohol)/sodium montmorillonite and polypropylene/clay nanocomposite, was not affected by compositing with nanoclays (*29*, *40*). However, the transparency of the chitosan/Nano-silver films was significantly ($P < 0.05$) decreased. This was mainly due to the fact that the structure of Nano-silver was not a layered structure like the other nanoclays and partly because Nano-silver was not evenly distributed throughout the polymer matrix. It is interesting to note that the standard deviation value of T_{660} of the chitosan/Nano-silver films is much greater than the others. This is indirect

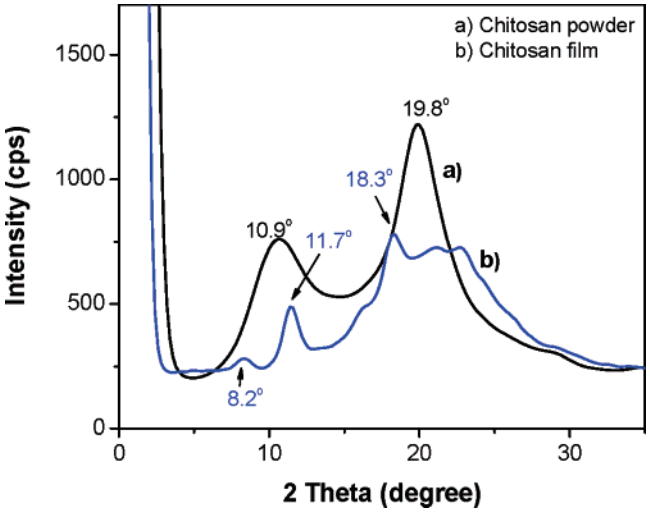

Figure 1. XRD patterns of chitosan powder and neat chitosan film.

evidence that Nano-silver particles are not evenly distributed in the polymer matrix.

XRD Analysis. Figure 1 shows the XRD patterns of pure chitosan powder and chitosan film. Chitosan powder showed characteristic peaks at $2\theta = 10.9°$ and 19.8°. The peaks correspond to a hydrated crystalline structure and an amorphous structure of chitosan, respectively (*41*, *42*). On the other hand, neat chitosan film showed characteristic peaks around $2\theta = 8°$, 11°, and 18°. The former two peaks indicated a hydrated crystalline structure, whereas the latter peak indicated an amorphous structure of chitosan (*41*, *42*). It is generally known that the structure of chitosan is strongly dependent on its processing treatment, such as dissolving, precipitation, and drying, as well as its origin and characteristics, such as degree of deacetylation and molecular weight (*43*). However, the crystalline structure of chitosan was not significantly affected through the film preparation as indicated by comparison of the XRD patterns.

XRD patterns of chitosan-based nanocomposite films are shown in **Figure 2**. XRD peaks of nanoclay were shifted from 7.0° to 4.8° for Na-MMT and from $2\theta = 4.9°$ to 4.56° for Cloisite 30B after formation of nanocomposite with chitosan; however, the degree of shift was dependent on the nanoclay used. These shifts indicated significant intercalation in the hybrid structure. More shift in the chitosan/Na-MMT film is probably due to higher compatibility of the Na-MMT clay than the organically modified MMT (Cloisite 30B) with chitosan matrix. It perhaps resulted in the interaction between Na^+ ions of the Na-MMT clay and the free hydroxyl groups of chitosan. Because of the hydrophilic and polycationic nature of chitosan in acidic media, this biopolymer has good miscibility with MMT and can easily intercalate into the interlayer by means of cationic exchange (*44*). The increase in the basal spacing, d_{001}, suggests the intercalation of chitosan in a monolayer disposition (*29*, *31*) and, additionally, indicates that Na-MMT is more compatible than Cloisite 30B with chitosan. This agrees with previously reported results that a hydrophilic unmodified MMT was more compatible with hydrophilic natural biopolymer than organically modified organophilic MMT (*45*, *46*).

Figure 2 also shows XRD patterns of chitosan/Nano-silver nanocomposite (NC) and chitosan/Ag-Ion NC films. In the case of Nano-silver powder-incorporated chitosan NC film (**Figure 2C**b), the crystalline structure of Nano-silver was not significantly affected, as shown by the XRD pattern of chitosan/Nano-silver composite films that still exhibited the peaks of neat chitosan film at $2\theta = 38°$ ($d_{001} = 111$ nm), 44° ($d_{001} = 200$ nm), 64° ($d_{001} = 220$ nm), and 77° ($d_{001} = 311$ nm), although they were decreased slightly compared with pristine Nano-silver powder (**Figure 2C**a). However, in the case of Ag-Ion-loaded chitosan NC film (**Figure 2D**b), the XRD peak shifted from $2\theta = 17.8°$ for pure Ag-Ion (**Figure 2B**a) to 20°, and most of the crystalline peaks of the Ag-Ion also disappeared. Together, these indicate significant intercalation and a phase change of Ag-Ion from a crystalline phase into an amorphous one in the hybrid structure and may be attributed to possible intercalations between Ag ions and free hydroxyl groups of chitosan.

Film Microstructure. Figure 3 shows SEM images of the cross-sectional surface of chitosan and chitosan-based nanocomposite films. The bright parts in the nanocomposite fractured films are the ends of the broken nanoparticles. SEM images for NC films with Cloisite 30B, Nano-silver, and Ag-Ion showed island−sea morphology; that is, the nanoparticles were dispersed throughout the chitosan matrix, whereas those with Na-MMT appeared to have intercalated or layered silicate morphology. In the case of NC films with Nano-silver, aggregated particles were observed in part of the film matrix (**Figure 3D**). This explains the results of the transparency measurements (T_{660}) of the films (**Table 1**); that is, the standard deviation for the T_{660} values of chitosan/Nano-silver films was much greater than those of other nanocomposite films.

Tensile Properties. Table 2 shows the results of thickness, TS, and *E* for chitosan and chitosan nanocomposite films. The thickness of the nanocomposite films was not significantly ($P > 0.05$) different from that of chitosan film; that is, thickness was not affected by compositing with the nanoparticles used. TS and *E* of chitosan films were 32.9 ± 0.7 MPa and 54.6 ± 3.0%, respectively. These values were in good agreement with previously reported values for chitosan films (*38*, *47*). TS of all the nanocomposite films increased significantly ($P < 0.05$), whereas *E*, for all except the chitosan/Cloisite 30B film, decreased significantly by compositing with nanoparticles. Such a reinforcing effect on chitosan film through compositing with nanoparticles was mainly attributed to a possible strain-induced alignment of the nanoparticle layers in the polymer matrix (*30*). This increase in toughness of hybrids containing evenly distributed nanoparticle layers in a polymer matrix has been frequently observed with various nanocomposites (*29*, *31*−*33*). The main reason for the increase in tensile strength in polymer/layered silicate clay nanocomposites is the strong interaction between polymer matrix and silicate layers via the formation of hydrogen bonds (*31*). The extent of the increase in TS depends directly upon the average length of the dispersed clay particles and, hence, the aspect ratio.

WVP. The WVP values, along with actual relative humidity conditions at the undersides of films during testing, of the chitosan and chitosan-based nanocomposite films are shown in **Table 3**. The WVP value of the chitosan film was (1.31 ± 0.07) × 10^{-12} kg·m/m²·s·Pa, which is in good agreement with the reported value of (1.34 ± 0.14) × 10^{-12} kg·m/m²·s·Pa (*38*). The WVP of the nanocomposite films decreased significantly ($P < 0.05$) by 25−30% depending on the nanoparticles used. The decrease in WVP of nanocomposite films is believed to be due to the presence of ordered dispersed nanoparticle layers with large aspect ratios in the polymer matrix (*48*, *49*). This forces water vapor traveling through the film to follow a tortuous path through the polymer matrix surrounding the nanoparticles, thereby increasing the effective path length for diffusion.

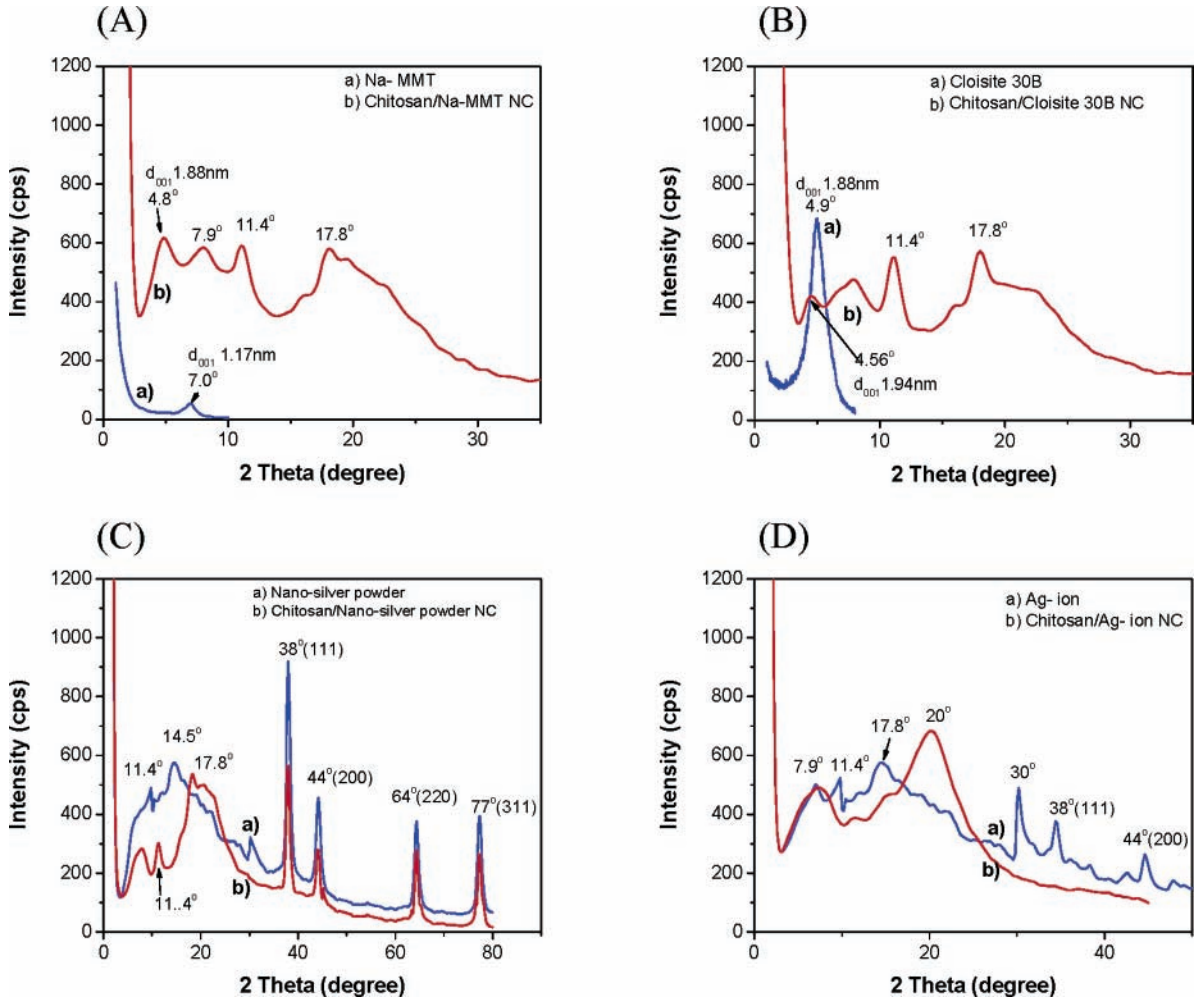

Figure 2. XRD patterns of nanoparticles and their respective chitosan-based nanocomposite films.

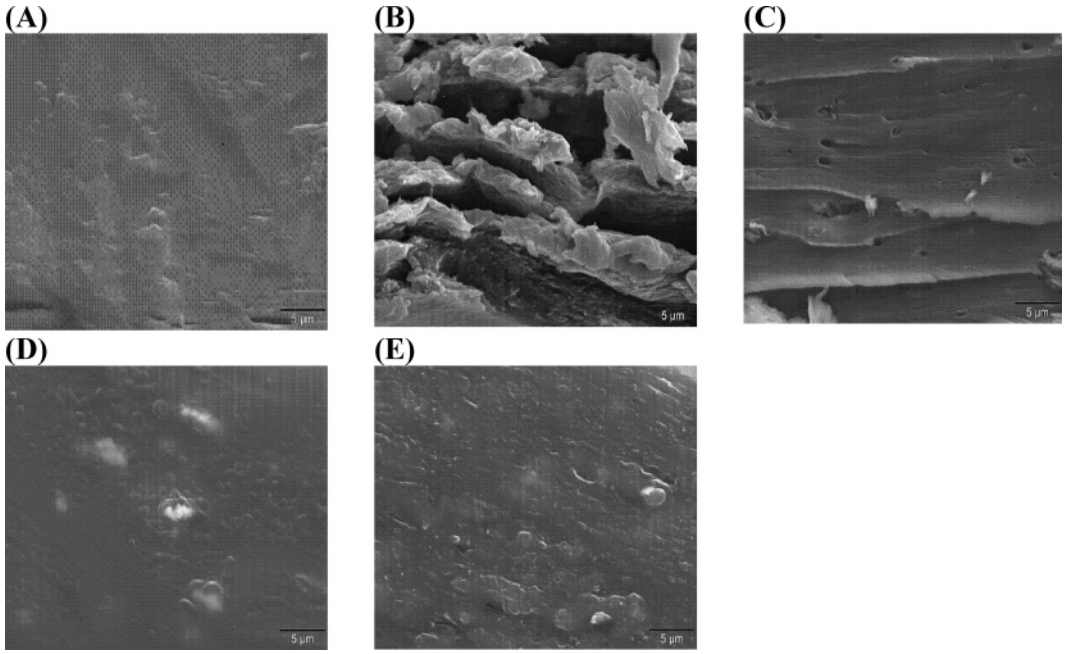

Figure 3. SEM of cross sections of films from chitosan and chitosan-based nanocomposites (magnification = 3500×): (**A**) neat chitosan; (**B**) chitosan/Na-MMT; (**C**) chitosan/Cloisite 30B; (**D**) chitosan/Nano-silver; (**E**) chitosan/Ag-Ion).

The observed decrease in WVP is of great importance in evaluating the nanocomposite films for use in food packaging, protective coatings, and other applications where efficient polymer barriers are needed. For these applications, the implications of a significant reduction in WVP means either increased barrier efficiency for a given film thickness or a reduction in thickness of the barrier layer for the same efficiency. Among the nanocomposite films tested, the chitosan/Cloisite 30B film

Table 2. Tensile Properties of Chitosan-Based Nanocomposite Films[a]

film type	thickness (μm)	TS (MPa)	E (%)
neat chitosan	64.0 ± 6.0a	32.9 ± 0.7b	54.6 ± 3.0ab
Na-MMT	70.0 ± 9.2a	35.1 ± 0.9ab	50.3 ± 11.7bc
Cloisite 30B	63.3 ± 2.3a	36.8 ± 3.3ab	66.3 ± 5.3a
Nano-silver	64.7 ± 9.0a	35.9 ± 1.9ab	46.3 ± 7.6bc
Ag-Ion	61.3 ± 5.0a	38.0 ± 3.4a	38.9 ± 1.4c

[a] Means of three replicates ± standard deviation. Any two means in the same column followed by the same letter are not significantly different from each other ($P > 0.05$) by Duncan's multiple-range test. TS, tensile strength; E, elongation at break.

was the lowest in WVP. The increase in water vapor barrier property may also have been due to the development of a polymeric composite structure with nanoparticles.

Although the WVP values of chitosan film decreased upon compositing with nanoparticles, they are still not comparable to those of widely used plastic films (*39*). The WVP (in kg·m/m^2·s·Pa) for various petroleum-based plastic films documented in the literature (*50*) is 4 orders of magnitude lower than that of the chitosan-based films tested. This indicates that the WVP of chitosan-based films needs further improvement to substitute for petroleum-based plastic films.

Contact Angle of Water. The contact angle (CA) of water is one of the basic wetting properties of packaging materials and is an indicator of the hydrophilic/hydrophobic properties of the material (*51*). Results of the initial contact angle of water measurements for the films are shown in **Table 3**. Usually, the more hydrophilic a material is, the lower the contact angle value it has. Contact angle measurement of the films studied indicated that, generally, hydrophilicity of chitosan-based nanocomposite films, except for the chitosan/Cloisite 30B film, decreased by compositing with nanoclays or a nanoparticle. This seems to be contradictory to the expected results that hydophilicity of films composited with Na-MMT increases (i.e., a decrease in CA) due to the hydrophilic nature of the nanoclay surface with Na^+ or Ca^{2+} ions, as well as the structure of clay, whereas that with Cloisite 30B decreases (i.e., an increase in CA) due to replacement of Na^+ in the interlayer region of MMT with hydrophobic alkylammonium, methyl tallow bis(2-hydroxyethyl) quaternary ammonium, endowing it wih hydrophobicity (*29*, *45*). This discrepancy needs to be studied further.

WS. WS, a measure of the resistance of a film sample to water, showed similar trends as CA measurements (**Table 3**). The WS of nanocomposite films composited with Na-MMT and Cloisite 30B was not affected significantly, but those composited with Nano-silver and Ag-Ion had increased WS, that is, decreased water resistance.

Antimicrobial Activity. Figure 4 shows a typical antimicrobial test result of chitosan-based films against *S. aureus* as determined by the disk method. As shown in the picture,

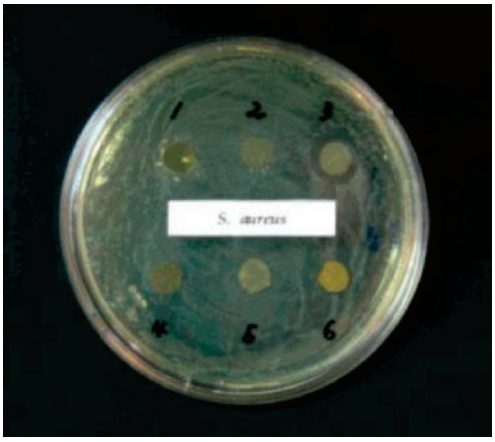

Figure 4. Photograph of antimicrobial test results of chitosan and chitosan-based nanocomposite films against *S. aureus*: (1) neat chitosan film; (2) chitosan/Na-MMT; (3) chitosan/Cloisite 30B; (4) chitosan/Nano-silver; (5) chitosan/Ag-Ion (5%); (6) chitosan/Ag-Ion (20%).

antimicrobial activity, determined by the diameter of the growth inhibition zone, was dependent on the test film used. The tests on all film samples were repeated using three other microorganisms, and the results are shown in **Table 4**. Generally, chitosan and chitosan/Na-MMT nanocomposite films did not show clear microbial inhibition zones, whereas Nano-silver- and Ag-Ion-incorporated nanocomposite films exhibited distinctive microbial inhibition zones against all four test microorganisms in the disk method. It is well-known that chitosan itself has antimicrobial activity due to its cationic property. This seemingly contradictory result for chitosan films is mainly due to the limits of detection of antimicrobial activity when using the disk method. The appearance and size of the clear zone in the disk method is mainly dependent on the ratio of disk area and size of inoculum, type of solid medium, and contact area. Of interest, Cloisite 30B-incorporated nanocomposite film exhibited antimicrobial activity against the two Gram-positive bacteria studied, *S. aureus* and *L. monocytogenes*, but did not show any antimicrobial activity against the two Gram-negative bacteria, *S. typhimurium* and *E. coli* O157:H7. In the case of Ag-Ion-incorporated films, the higher the concentration of Ag-Ion incorporated, the higher the antimicrobial activity obtained.

To confirm the above antimicrobial test results of chitosan films, a quantitative test, that is, a viable cell colony count method, was performed, and the results are shown in **Figure 5**. Like the disk test result, the antimicrobial activity of chitosan films varied distinctively depending on films and microorganisms tested. In the case of Gram-positive bacteria (i.e., *S. aureus* and *L. monocytogenes*), all chitosan-based films, including control chitosan and chitosan nanocomposite films, showed antimicrobial activity. In particular, nanocomposite films incorporated with Ag (Nano-silver and Ag-Ion) and Cloisite 30B-

Table 3. Water Vapor Barrier and Water Resistance Properties of Chitosan-Based Nanocomposite Films[a]

film type	MC (%, wb)	WVP ($\times 10^{-12}$ kg·m/m^2·s·Pa)	RH_i (%)	CA (deg)	WS (%)
neat chitosan	27.1 ± 0.8a	1.31 ± 0.07a	76.2 ± 1.4c	45.6 ± 0.2c	13.6 ± 1.1b
Na-MMT	26.4 ± 0.4a	0.98 ± 0.15bc	78.8 ± 0.6a	47.4 ± 0.2b	12.5 ± 0.8b
Cloisite 30B	24.3 ± 0.2b	0.92 ± 0.03c	78.2 ± 0.2ab	43.4 ± 1.3d	13.2 ± 1.0b
Nano-silver	24.5 ± 0.0b	0.95 ± 0.12bc	78.1 ± 0.2ab	48.5 ± 1.1b	14.1 ± 0.8ab
Ag-Ion	22.3 ± 0.3c	0.96 ± 0.05bc	77.3 ± 0.4bc	50.4 ± 1.0a	15.4 ± 0.6a

[a] Means of three replicates ± standard deviation. Any two means in the same column followed by the same letter are not significantly different from each other ($P > 0.05$) by Duncan's multiple-range test. MC, moisture content; WVP, water vapor permeability; RH_i, actual relative humidity value underneath the film covering the WVP measuring cup; CA, contact angle of water drop; WS, water solubility.

Table 4. Antimicrobial Activity[a] of the Chitosan Nanocomposite Films As Observed by an Agar Diffusion Assay on Plate Medium[b]

	film type					
test organism	neat chitosan	Na-MMT	Cloisite 30B	Nano-silver	Ag-Ion$_5$[c]	Ag-Ion$_{20}$[c]
S. aureus ATCC-14458	–	–	++	+	+	+
L. monocytogenes ATCC-19111	–	–	+	+	+	++
S. typhimurium ATCC-14028	–	–	–	+	+	++
E. coli O157:H7 ATCC-11775	–	–	–	+	+	++

[a] –, no inhibition; +, clear zone of 6–8 mm; ++, clear zone of 8–10 mm. [b] Culture medium: TSA (tryptic soy agar, Difco Lab.), incubation temperature = 37 °C. [c] Ag-Ion$_5$ and Ag-Ion$_{20}$, Ag-Ion concentration of 5 and 20% (w/w of chitosan), respectively.

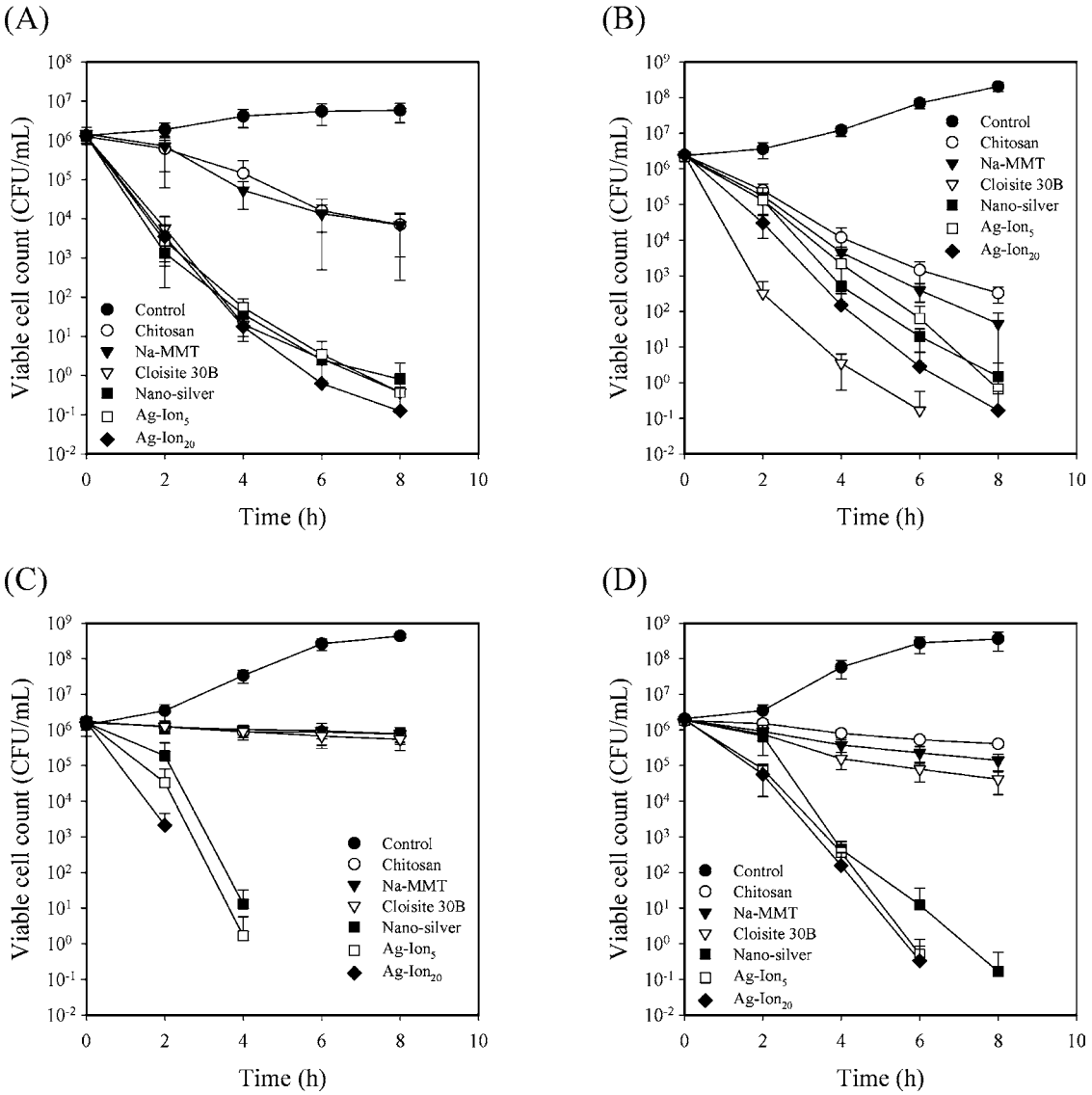

Figure 5. Effect of antimicrobial activity of chitosan and chitosan-based nanocomposite films on broth cultures of (**A**) *S. aureus*, (**B**) *L. monocytogenes*, (**C**) *S. typhimurium*, and (**D**) *E. coli* O157:H7.

incorporated films showed significantly lower levels of viable CFU. *S. aureus* treated with Ag-incorporated films decreased by >6 log cycles within 8 h of cultivation compared to the control without films, whereas *L. monocytogenes* decreased most rapidly in the presence of Cloisite 30B-incorporated film followed by Ag-Ion$_{20}$-, Nano-silver-, and Ag-Ion$_5$-incorporated films. Neat chitosan and Na-MMT- and Cloisite 30B-incorporated films each demonstrated a bacteriostatic effect against Gram-negative bacteria (i.e., *S. typhimurium* and *E. coli* O157:H7), but Ag-incorporated films exhibited distinct bactericidal effects. No viable CFU of *S. typhimurium* were observed after 6 h of cultivation with Ag-incorporated films in the decreasing order Ag-Ion$_{20}$ > Ag-Ion$_5$ > Nano-silver. In the same way, no viable CFU of *E. coli* O157:H7 were observed after 8 h of cultivation with Ag-incorporated films, indicating a ≈8 log cycle reduction effect compared with the control.

The antimicrobial activity of neat chitosan and Na-MMT-incorporated films may be contributed by the combined effect of chitosan and organic acid (i.e., acetic acid), whereas the increased antimicrobial activity of Ag-incorporated films may be increased by high infiltration of the Ag component with high bactericidal effect. Ag ions reportedly adhere to the negatively charged bacteria cell wall, changing the cell wall permeability. This action coupled with protein denaturation induces cell lysis

and death (*52*). The antimicrobial activity of Ag-Ion is also related to its ability to modify the DNA replication mechanisms as well as to cause abnormalities in the size, cytoplasmic contents, cell membrane, and outer cell layers of sensitive cells (*53*). Overall comparison of the microbial reduction rates in the present study revealed Gram-negative bacteria to be more susceptible to the antimicrobial effects of Ag ions than Gram-positives, presumably due to their thinner murine wall, which may allow more rapid absorption of the ions into the cell (*54*, *55*).

Interestingly, Cloisite 30B-incorporated film showed significantly higher antimicrobial activity against *S. aureus* and *L. monocytogenes* than Na-MMT-incorporated film, even though the basic structure of MMT is the same for both. This may be attributed to the antimicrobial activity of the quaternary ammonium group in the silicate layer of the Cloisite 30B-incorporated film. The effectiveness of such groups bearing alkyl substituents in disrupting bacterial cell membranes and causing cell lysis has been well documented in the literature (*56*−*59*). However, varied resistance of Gram-negative bacteria to quaternary ammonium compounds has been previously observed (*60*, *61*) and supports the present results for *S. typhimurium* and *E. coli* O157:H7.

Conclusions. Four different types of chitosan-based nanocomposite films were developed, and their film properties and antimicrobial functions were tested. By compositing with nanoparticles (such as unmodified and organically modified montmorillonites, Nano-silver, and silver zeolite), mechanical and water vapor barrier properties of chitosan films were increased significantly ($P < 0.05$) compared with those of control chitosan films, and varying degrees of antimicrobial activity were observed depending on the nanoparticles used. These results suggest a potential application of nanotechnology in the development of natural biopolymer-based biodegradable packaging materials with additional bioactive function.

LITERATURE CITED

(1) Kester, J. J.; Fennema, O. R. Edible films and coatings: a review. *Food Technol*. **1986**, *40* (12), 47−59.

(2) Guilbert, S. Technology and application of edible protective films. In *Food Packaging and Preservation, Theory and Practice*; Mathlouthi M., Ed.; Elsevier Applied Science Publishing: London, U.K., 1986; pp 371−394.

(3) Debeaufort, F.; Quezada-Gallo, J.-A.; Voilley, A. Edible films and coatings: tomorrow's packagings: a review. *Crit. Rev. Food Sci*. **1998**, *38*, 299−313.

(4) Krochta, J. M.; De Mulder-Johnston, C. Edible and biodegradable polymer films: challenges and opportunities. *Food Technol*. **1997**, *51* (2), 61−74.

(5) Wong, D. W. S.; Camirand, W. M.; Pavlath, A. E. Development of edible coatings for minimally processed fruits and vegetables. In *Edible Coatings and Films to Improve Food Quality*; Krochta, J. M., Baldwin, E. A., Nisperos-Carriedo, M. O., Eds.; Technomic Publishing: Lancaster, PA, 1994; pp 65−88.

(6) Baldwin, E. A. Edible coatings for fresh fruits and vegetables: Past, present and future. In *Edible Coatings and Films to Improve Food Quality*; Krochta, J. M., Baldwin, E. A., Nisperos-Carriedo, M. O., Eds.; Technomic Publishing: Lancaster, PA, 1994; pp 25−64.

(7) Gennadios, A.; Hanna, M. A.; Kurth, L. B. Application of edible coatings on meats, poultry and seafoods: a review. *Lebensm. Wiss. Technol*. **1997**, *30*, 337−350.

(8) Han, J. H. Antimicrobial food packaging. *Food Technol*. **2000**, *54* (3), 56−65.

(9) Mei, Y.; Zhao, Y. Barrier and mechanical properties of milk protein-based edible films containing nutraceuticals. *J. Agric. Food Chem*. **2003**, *51*, 1914−1918.

(10) Park, S.-I.; Zhao, Y. Incorporation of a high concentration of mineral or vitamin into chitosan-based films. *J. Agric. Food Chem*. **2004**, *52*, 1933−1939.

(11) Labuza, T. P.; Breene, W. M. Applications of active packaging for improvement of shelf-life and nutritional quality of fresh and extended shelf-life foods. *J. Food Process. Preserv.* **1989**, *13*, 1−69.

(12) Cha, D. S.; Chinnan, M. S. Biopolymer-based antimicrobial packaging: a review. *Crit. Rev. Food Sci. Nutr*. **2004**, *44*, 223−237.

(13) Cagri, A.; Ustunol, Z.; Ryser, E. T. Antimicrobial edible films and coatings. *J. Food Prot*. **2004**, *67*, 833−848.

(14) Hernandez, E. Edible coatings from liquid and resins. In *Edible Coatings and Films to Improve Food Quality*; Krochta, J. M., Baldwin, E. A., Nisperos-Carriedo, M. O., Eds.; Technomic Publishing: Lancaster, PA, 1994; pp 279−303.

(15) Avena-Bustillos, R. J.; Krochta, J. M. Water vapor permeability of caseinate-based edible films as affected by pH, calcium crosslinking and lipid content. *J. Food Sci*. **1993**, *58*, 904−907.

(16) McHugh, T. H.; Krochta, J. M. Water vapor permeability properties of edible whey protein−lipid emulsion films. *J. Am. Oil Chem. Soc*. **1994**, *71*, 307−312.

(17) Lai, H. M.; Padua, G. W.; Wei, L. S. Properties and microstructure of zein sheets plasticized with palmitic and stearic acid. *Cereal Chem*. **1997**, *74*, 83−90.

(18) Shellhammer, T. H.; Krochta, J. M. Whey protein emulsion film performance as affected by lipid type and amount. *J. Food Sci*. **1997**, *62*, 390−394.

(19) Morillon, V.; Debeaufort, F.; Blond, G.; Capelle, M.; Voilley, A. Factors affecting the permeability of lipid-based edible films: a review. *Crit. Rev. Food Sci. Nutr*. **2002**, *42*, 67−89.

(20) Rhim, J. W. Increase in water vapor barrier properties of biopolymer-based edible films and coatings by compositing lipid materials. *Food Sci. Biotechnol*. **2004**, *13*, 528−535.

(21) Rhim, J. W.; Gennadios, A.; Fu, D.; Weller, C. L.; Hanna, M. A. Properties of ultraviolet irradiated protein films. *Lebensm. Wiss. Technol*. **1999**, *32*, 129−133.

(22) Banerjee, R.; Chen, H.; Wu, J. Milk protein-based edible film mechanical strength changes due to ultrasound process. *J. Food Sci*. **1996**, *61*, 824−828.

(23) Gennadios, A.; Ghorpade, V. M.; Weller, C. L.; Hanna, M. A. Heat curing of soy protein films. *Trans. ASAE* **1996**, *39*, 575−579.

(24) Brandenburg, A. H.; Weller, C. L.; Testin, R. F. Edible films and coatings from soy protein. *J. Food Sci.* **1993**, *58*, 1086−1089.

(25) Ghorpade, V. M.; Li, H.; Gennadios, A.; Hanna, M. A. Chemically modified soy protein films. *Trans. ASAE* **1995**, *38*, 1805−1808.

(26) Galietta, G.; Gioia, L. D.; Guilbert, S.; Cuq, B. Mechanical and thermomechanical properties of films based on whey proteins as affected by plasticizer and crosslinking agents. *J. Dairy Sci*. **1998**, *81*, 3123−3130.

(27) Fischer, S.; Vlieger, J.; Batenburg, L.; Fischer, H.; Kock, T. 'Green' nano-composite materials−new possibilities for bioplastics. *Materialen* **2000**, *16* (3−7), 12.

(28) Lagaly, G. Introduction: from clay mineral−polymer interactions to clay mineral-polymer nanocomposites. *Appl. Clay Sci*. **1999**, *15*, 1−9.

(29) Alexandre, M.; Dubois, P. Polymer-layered silicate nanocomposites: preparation, properties and use of a new class of materials. *Mater. Sci. Eng*. **2000**, *28*, 1−63.

(30) Giannelis, E. P. Polymer layered silicate nanocomposites. *Adv. Mater*. **1996**, *8*, 29−35.

(31) Sinha Ray, S.; Okamoto, M. Polymer/layered silicate nanocomposites: a review from preparation to processing. *Prog. Polym. Sci*. **2003**, *28*, 1539−1641.

(32) Pandey, J. K.; Kumar, A. P.; Misra, M.; Mohanty, A. K.; Drzal, L. T.; Singh, R. P. Recent advances in biodegradable nanocomposites. *J. Nanosci. Nanotechnol*. **2005**, *5*, 497−526.

(33) Sinha Ray, S.; Bousmina, M. Biodegradable polymers and their layered silicate nanocomposites: in greening the 21st century materials world. *Prog. Mater. Sci*. **2005**, *50*, 962−1079.
(34) Schmidt, D.; Shah, D.; Giannelis, E. P. New advances in polymer/layered silicate nanocomposites. *Curr. Opin. Solid State Mater. Sci*. **2002**, *6*, 205−212.
(35) Yu, Y. H.; Lin, C. Y.; Yeh, J. M.; Lin, W. H. Preparation and properties of poly(vinyl alcohol)−clay nanocomposite materials. *Polymer* **2003**, *44*, 3553−3560.
(36) Del Nobile, M. A.; Cannaris, M.; Altieri, C.; Sinigaglia, M.; Favia, P.; Iacoviello, G.; D'Agostino, R. Effect of Ag-containing nano-composite active packaging system on survival of *Alicyclobacillus* acidoterrestris. *J. Food Sci*. **2004**, *69*, E379−E383.
(37) Ruan, D.; Zhang, L.; Zhang, Z.; Xia, X. Structure and properties of regenerated cellulose/tourmaline nanocrystal composite films. *J. Polym. Sci., Part B: Polym. Phys*. **2003**, *42*, 367−373.
(38) Rhim, J. W.; Weller, C. L.; Ham, K. S. Characteristics of chitosan films as affected by the type of solvent acid. *Food Sci. Biotechnol*. **1998**, *7*, 263−268.
(39) Gennadios, A.; Weller, C. L.; Gooding, C. H. Measurement errors in water vapor permeability of highly permeable, hydrophilic edible films. *J. Food Eng*. **1994**, *21*, 395−409.
(40) Strawhecher, K. E.; Manias, E. Structure and properties of poly(vinyl alcohol)/Na^+-montmorillonite nanocomposites. *Chem. Mater*. **2000**, *12*, 2943−2949.
(41) Ogawa, K.; Hirano, S.; Miyanishi, T.; Yui, T.; Watanabe, T. A new polymorph of chitosan. *Macromolecules* **1984**, *17*, 973−975.
(42) Wang, S. F.; Shen, L.; Zhang, W. D.; Tong, Y. J. Preparation and mechanical properties of chitosan/carbon nanotubes composites. *Biomacromolecules* **2005**, *6*, 3067−3072.
(43) Jaworska, M.; Sakurai, K.; Gaudon, P.; Guibal, E. Influence of chitosan characteristics on polymer properties. I. Crystallographic properties. *Polym. Int*. **2003**, *2*, 198−205.
(44) Darder, M.; Colilla, M.; Ruiz-Hitzky, E. Biopolymer−clay nanocomposites based on chitosan intercalated in montmorillonite. *Chem. Mater*. **2003**, *15*, 3774−3780.
(45) Xu, Y.; Zhou, J.; Hanna, M. A. Melt-intercalated starch acetate nanocomposite foams as affected by type of organoclay. *Cereal Chem*. **2005**, *82*, 105−110.
(46) Park, H. M.; Misra, M.; Drzal, L. T.; Mohanty, A. K. "Green" nanocomposites from cellulose acetate bioplastic and clay: effect of eco-friendly triethyl citrate plasticizer. *Biomacromolecules* **2004**, *5*, 2281−2288.
(47) Butler, B. L.; Vergano, P. J.; Testin, R. F.; Bunn, J. M.; Wiles, J. L. Mechanical and barrier properties of edible chitosan films as affected by composition and storage. *J. Food Sci*. **1996**, *61*, 953−956.
(48) Yano, K.; Usuki, A.; Okad, A. Synthesis and properties of polyimide−clay hybrid films. *J. Polym. Sci., Part A: Polym. Chem*. **1997**, *35*, 2289−2294.
(49) Cussler, E. L.; Highes, S. E.; Ward, W. J.; Aris, R. Barrier membranes. *J. Membr. Sci*. **1998**, *38*, 161−174.
(50) Salamie, M. Polyethylene, low density. In *The Wiley Encyclopedia of Packaging Technology*; Bakker, M., Ed.; Wiley: New York, 1986; pp 514−523.
(51) Han, J. H.; Krochta, J. M. Wetting properties and water vapor permeability of whey protein-coated paper. *Trans. ASAE* **1999**, *42* (5), 1375−1382.
(52) Lin, Y. E.; Vidic, R. D.; Stout, J. E.; Yu, V. L. Individual and combined effects of copper and silver ions on inactivation of *Legionella pneumophila*. *Water Res*. **1996**, *30*, 1905−1913.
(53) Russell, A. D.; Hugo, W. B. Antimicrobial activity and action of silver. *Prog. Med. Chem*. **1994**, *31*, 351−358.
(54) Schierholz, J. M.; Lucas, L. J.; Rump, A.; Pulverez, G. Efficacy of silver-coated medical device. *Rev. J. Hosp. Inf*. **1998**, *40*, 257−262.
(55) Gray, J. E.; Norton, P. R.; Alnouno, R.; Marolda, C. L.; Valvano, M. A.; Griffiths, K. Biological efficacy of electroless-deposited silver on plasma activated polyurethane. *Biomaterials* **2003**, *24*, 2759−2765.
(56) Hugo, W. B.; Russel, A. D. Types of antimicrobial agents. In *Principles and Practice of Disinfection, Preservation and Sterilization*; Russel, A. D., Hugo, W. B., Ayliffe, G. A. J., Eds.; Blackwell Scientific Publications: Oxford, U.K., 1992; pp 7-68.
(57) Kim, C. H.; Choi, J. W.; Chun, H. J.; Choi, K. S. Synthesis of chitosan derivatives with quaternary ammonium salt and their antibacterial activity. *Polym. Bull.* **1997**, *38*, 387−393.
(58) Gottenbos, B.; Van der Mei, H. C.; Klatter, F.; Nieuwenhuis, P.; Busscher, H. J. In vitro and in vivo antimicrobial activity of covalently coupled quaternary ammonium silane coatings on silicone rubber. *Biomaterials* **2002**, *23*, 1417−1423.
(59) Kim, J. Y.; Lee, J. K.; Lee, T. S.; Park, W. H. Synthesis of chitooligosaccharide derivative with quaternary ammonium group and its antimicrobial activity against *Streptococcus mutans*. *Int. J. Biol. Macromol*. **2003**, *32*, 23−27.
(60) Winniczuk, P. P.; Parish, M. E. Minimum inhibitory concentrations of antimicrobials against microorganisms related to citrus juice. *Food Microbiol*. **1997**, *14*, 373−381.
(61) Cords, B. E.; Dychdala, G. R. Sanitizers: halogens, surface-active agents, and peroxides. In *Antimicrobials in Foods*; Davidson, P. M., Sofos, J. N., Branen, A. L., Eds.; CRC Press: Boca Raton, FL, 2005; pp 507−572.

Received for review March 8, 2006. Revised manuscript received May 17, 2006. Accepted May 31, 2006. This work was supported by Grant R01-2003-000-10389-0 from the Basic Research Program of the Korea Science & Engineering Foundation and partially supported by Michigan Agricultural Experiment Station.

JF060658H